Human Molecular Genetics, 2013, Vol. 22, No. 20 **4224–4232**
doi:10.1093/hmg/ddt274
Advance Access published on June 17, 2013

PLEKHG5 deficiency leads to an intermediate form of autosomal-recessive Charcot–Marie–Tooth disease

Hamid Azzedine[1,†], Petra Zavadakova[1,†], Violaine Planté-Bordeneuve[2], Maria Vaz Pato[3], Nuno Pinto[3], Luca Bartesaghi[1], Jennifer Zenker[1], Olivier Poirot[1], Nathalie Bernard-Marissal[1], Estelle Arnaud Gouttenoire[1], Romain Cartoni[1], Alexandra Title[1], Giulia Venturini[1], Jean-Jacques Médard[1], Edward Makowski[4], Ludger Schöls[5], Kristl G. Claeys[6,7], Claudia Stendel[7], Andreas Roos[6], Joachim Weis[6], Odile Dubourg[8], José Leal Loureiro[11,12], Giovanni Stevanin[9,10], Gérard Said[13], Anthony Amato[14], Jay Baraban[4], Eric LeGuern[9], Jan Senderek[15,†,*], Carlo Rivolta[1,†] and Roman Chrast[1,†,*]

[1]Department of Medical Genetics, University of Lausanne, CH-1005 Lausanne, Switzerland [2]Service de Neurologie, CHU Henri Mondor, 94000 Créteil, France [3]CICS-Health Science Research Centre, Universidade da Beira Interior, 6200-506 Covilhã, Portugal [4]Solomon H. Snyder Department of Neuroscience, John Hopkins University, Baltimore, MD 21205, USA [5]Department of Neurodegenerative Disease, Hertie-Institute for Clinical Brain Research and Center for Neurology, 72076 Tübingen, Germany [6]Institute of Neuropathology and [7]Department of Neurology, University Hospital RWTH Aachen, 52074 Aachen, Germany [8]Centre de reference des maladies neuromusculaires, Assistance Publique-Hôpitaux de Paris, [9]Centre de Recherche de l'Institut du Cerveau et de la Moelle épinière (Inserm/UPMC 975; CNRS 7225) and Departement of Genetics, Assistance Publique-Hôpitaux de Paris and [10]Neurogenetics Group, Ecole Pratique des Hautes Etudes, CHU Pitié-Salpêtrière, 75013 Paris, France [11]UnIGENe and Centro de Genética Preditiva e Preventiva, Institute for Molecular and Cellular Biology, 4050 Porto, Portugal [12]Serviço de Neurologia, Centro Hospitalar entre Douro e Vouga, 4520-211 Santa Maria da Feira, Portugal [13]Department of Neurology, Pitié-Salpêtrière Hospital, Assistance Publique-Hôpitaux de Paris, University Pierre et Marie Curie, 75013 Paris, France [14]Department of Neurology, Brigham and Women's Hospital, Harvard Medical School, Boston, MA 02115, USA [15]Department of Neurology, Friedrich-Baur-Institute, Ludwig-Maximilian-University, 81377 Munich, Germany

Received May 6, 2013; Revised and Accepted June 6, 2013

Charcot–Marie–Tooth disease (CMT) comprises a clinically and genetically heterogeneous group of peripheral neuropathies characterized by progressive distal muscle weakness and atrophy, foot deformities and distal sensory loss. Following the analysis of two consanguineous families affected by a medium to late-onset recessive form of intermediate CMT, we identified overlapping regions of homozygosity on chromosome 1p36 with a combined maximum LOD score of 5.4. Molecular investigation of the genes from this region allowed identification of two homozygous mutations in *PLEKHG5* that produce premature stop codons and are predicted to result in functional null alleles. Analysis of *Plekhg5* in the mouse revealed that this gene is expressed in neurons and glial cells of the peripheral nervous system, and that knockout mice display reduced nerve conduction velocities that are comparable with those of affected individuals from both families. Interestingly, a homozygous *PLEKHG5* missense mutation was previously reported in a recessive form of severe childhood onset lower motor neuron disease (LMND) leading to loss of the ability to walk and need for respiratory assistance. Together, these observations indicate that different mutations in *PLEKHG5* lead to clinically diverse outcomes (intermediate CMT or LMND) affecting the function of neurons and glial cells.

*To whom correspondence should be addressed. Tel: + 49 8951607415; Fax: +49 8951607416; Email: jan.senderek@med.uni-muenchen.de (J.S.); Tel: +41 216925450; Fax: +41 216925455; Email: roman.chrast@unil.ch (R.C.)
†These authors contributed equally to this work.

INTRODUCTION

Hereditary motor and sensory neuropathy (HMSN), also known as Charcot–Marie–Tooth disease (CMT), is the most frequent inherited neurological disorder with a prevalence of 1 in 2500 (1). CMT affects both sensory and motor peripheral nerves and is clinically characterized by distal and symmetric muscle atrophy in lower limbs and hands, foot deformities, distal sensory loss and decreased or absent tendon reflexes (2,3). Two major types have been distinguished on the basis of electrophysiological criteria: a demyelinating form (HMSN type I or CMT1) with motor nerve conduction velocities (MNCVs) of the median nerve lower than 38 m/s and an axonal form (HMSN type II or CMT2) in which MNCVs are normal or only slightly reduced (>40 m/s), while amplitudes of motor and sensory action potentials are significantly decreased (4–6). Histological features reflect these findings: in CMT1, peripheral nerve pathology shows defects of myelinating Schwann cells (SC), responsible for decreased nerve conduction, whereas in CMT2 the number of large caliber axons is reduced, leading to decreased motor and sensory action potentials. A third group of CMTs with MNCVs between 25 and 45 m/s is considered as intermediate (5,7,8). In this group of CMTs, histology shows the coexistence of glial (demyelination, onion bulb formation) and axonal (degeneration of large caliber axons and regenerative sprouting) defects (9,10).

While recent progress has allowed identification of more than 40 genes in various forms of CMT, there is still a relatively large fraction of cases for which molecular diagnosis cannot be established (11). As part of the effort to identify additional CMT-causing genes, we analyzed two consanguineous multiplex families presenting with an autosomal-recessive form of intermediate CMT and identified two homozygous mutations in *PLEKHG5*. These genetic data together with the characterization of the mice with disrupted *Plekhg5* clearly indicate that in addition to previously reported lower motor neuron disease (LMND) (12), mutations in *PLEKHG5* are also causing an intermediate CMT.

RESULTS

Identification of mutations in *PLEKHG5* in two families affected with an intermediate CMT

Two consanguineous multiplex families affected by an autosomal-recessive form of intermediate CMT were studied. The first family (221) originated from Portugal and comprised two affected and four unaffected siblings born to healthy parents who were first cousins. In the second family (NP72) of Moroccan origin, four out of eight siblings born to healthy parents with first-degree consanguinity were affected. Affected individuals had limb muscle weakness and atrophy, foot deformities, moderately decreased nerve conduction velocities, loss of large myelinated fibers and thin myelination seen on nerve biopsy (Fig. 1, Table 1). No signs of brain involvement were observed. In four of the five characterized affected individuals, the age of onset was between the second and fifth decade and one patient had earlier disease onset at the age of 7 years.

To identify the gene responsible for this characteristic form of recessive CMT, we performed genome-wide homozygosity mapping in both families. In family 221, microsatellite genotyping was performed with a set of ∼400 markers from the ABI-Prism linkage mapping set v2 revealing a few regions of homozygosity in the affected individuals, including an ∼10 Mb region at the 1p-telomere (Fig. 1 and Supplementary Material, Fig. S1). For family NP72, we used a set of ∼600 000 SNPs from the Illumina Human 660W-Quad array and mapping identified only one homozygous region genome-wide. This was a 1.52 Mb stretch on chromosome 1, which was common to all affected individuals and absent in the healthy members of the pedigree. Haplotype reconstruction revealed that two ancestral recombination events delimited the autozygous region in this latter family (Fig. 1). The 1.52 Mb autozygous region identified in family NP72 completely overlapped with the chromosome 1p-tel region of interest found in family 221. Combined parametric multipoint linkage analysis in both families [Merlin software (13), autosomal-recessive inheritance] confirmed these findings and assigned a max LOD score of 5.4 (LODmax = 1.9 and 3.5 for families 221 and NP72, respectively) to the shared region of homozygosity (Supplementary Material, Fig. S1). The critical interval contained 25 annotated genes (Fig. 2). Further analysis revealed that, according to data that we had generated previously (14), only two of them, *PLEKHG5* (MIM 611101) and *GPR153* (MIM 614269), had an expression profile compatible with genes playing a role in peripheral nerve development and function. Their Sanger sequencing (including coding exons and flanking intronic regions) in affected subjects revealed a homozygous 1 bp deletion in exon 3 of *PLEKHG5* (NM_198681.3:c.269delC) in family 221 leading to a frameshift and premature termination codon (NP_941374.2:p.Pro90Hisfs*45) and a homozygous 7 bp duplication (NM_198681.3:c.1143_1149dup [tgaagac]) in exon 10 of *PLEKHG5* directly introducing a stop codon (NP_941374.2:p.Glu384*) in family NP72 (Fig. 2). Parents for whom the DNA was available were heterozygotes for the mutations, and unaffected siblings were either heterozygotes or presented no mutations (Fig. 1). Neither c.269delC nor c.1143_1149dup were detected in controls (79 North African and 339 European, and 100 North African and 49 European subjects, respectively). Moreover, these mutations were absent from the dbSNP and the Exome Sequencing Project databases.

Pattern of expression of *Plekhg5* suggests its role in neurons and glial cells

PLEKHG5 was previously shown to be expressed in human spinal cord, brain and peripheral nerves (12), while the expression of its mouse and rat orthologue, *Plekhg5*, was detected in the brain (15,16). We have confirmed and extended these findings using samples from various regions of adult (2-month-old) mouse nervous system. Quantitative PCR data revealed the highest level of expression of *Plekhg5* in the brain and in the sciatic nerve endoneurium (Fig. 3A). Interestingly, the endoneurial expression of *Plekhg5* was dynamically regulated during development with the highest level at postnatal days 10–14 (Fig. 3B). This expression profile suggested its role in PNS myelination (14,17). We therefore evaluated the expression of *Plekhg5* in SC and found that both primary purified mouse SC and the mouse SC line MSC80 expressed *Plekhg5* (Fig. 3C). The

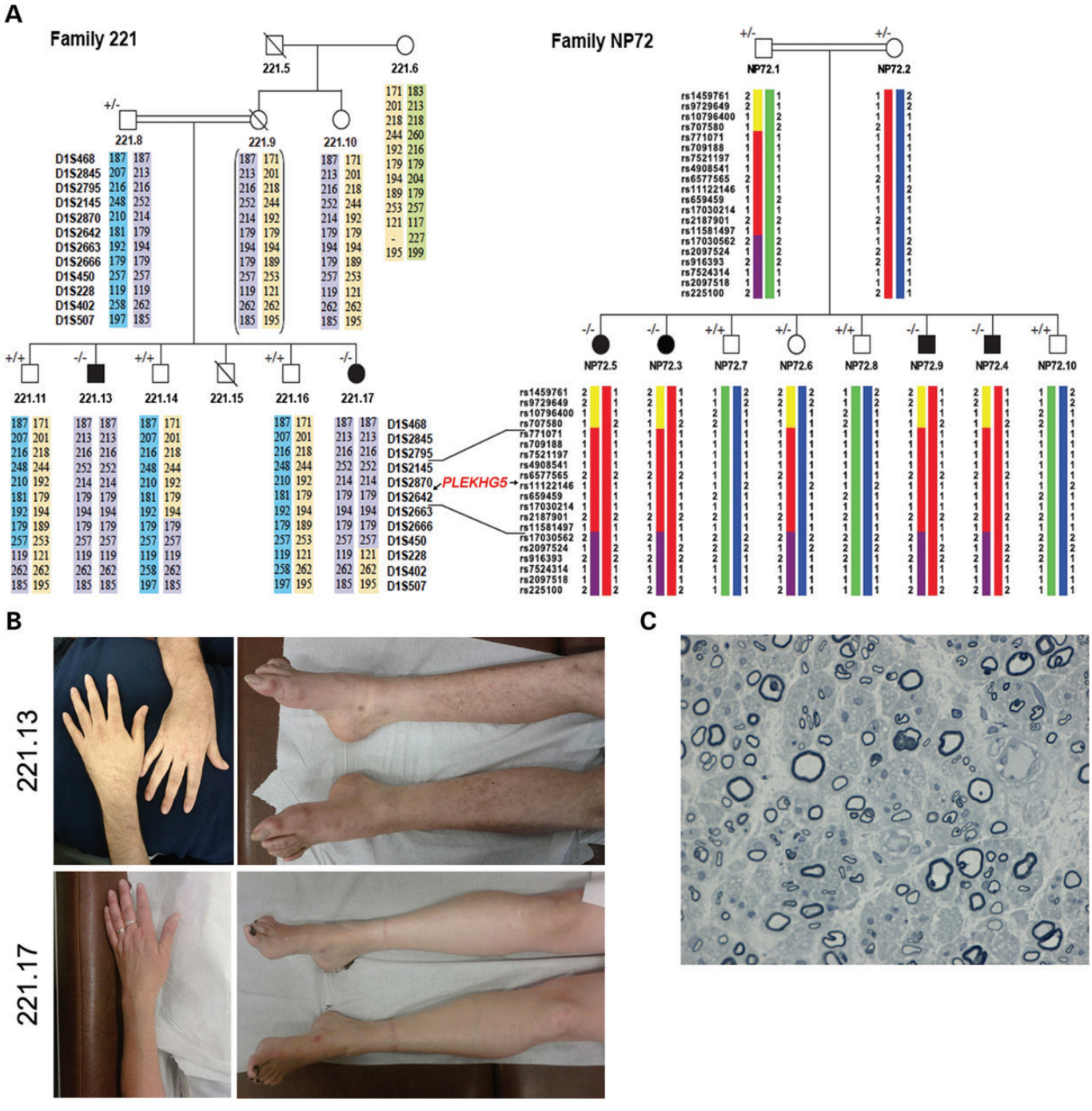

Figure 1. Characterization of two families affected with an intermediate form of CMT. (**A**) Haplotype reconstruction for 20 SNPs and 12 microsatellite markers of the chromosome 1p36 region in families 221 and NP72. Microsatellite and SNP markers are ordered from telomere (top) to centromere (bottom) and show overlapping segments of autozygosity. Deduced haplotypes of the mother of the siblings in family 221 are bracketed. The critical region of segregation is defined by ancestral recombination events revealed by haplotype reconstruction in family NP72. +, wild-type allele; -, mutation. (**B**) Pes cavus deformity is evident in both affected individuals from family 221. The distal amyotrophy is more pronounced in lower than in upper limbs. (**C**) Transverse section of sural nerve biopsy sample of individual NP72.5 (Thionin-stained semi-thin section of a glutaraldehyde fixed, osmium tetroxidepost-fixed, epon-embedded nerve biopsy specimen; ×400 magnification). Most axons are surrounded by a disproportionally thin myelin sheath. In addition, myelinated nerve fiber density is reduced to about 70% of normal with predominant loss of larger fibers.

temporal and spatial expression pattern of *Plekhg5* in neurons and glial cells is in agreement with its possible role in the pathophysiology of an intermediate CMT subtype affecting both neurons and SC.

Plekhg5$^{\Delta Ex11\text{-}Ex17/\Delta Ex11\text{-}Ex17}$ mice develop mild neuropathy

In order to gain insight into the consequences of disrupted PLEKHG5 function, we decided to use recently generated

Table 1. Summary of clinical findings in families NP72 and 221

Family	NP72			221	
Patient	NP72.4	NP72.5	NP72.9	221.13	221.17
Gender	M	F	M	M	F
Age at onset (years)	28	44	30	7	20
Age at last examination (years)	43	53	47	51	42
Distal weakness					
UL[a]	+	++	++	++	+
LL[b]	++	+++	+++	++	+
Distal muscle atrophy[c]					
UL	++	++	++	++	−
LL	+++	++	++	++	−
Involvement of proximal muscles[d]					
UL	−	+	+	+	−
LL	−	++	+	+	−
Foot deformity[e]	+/ht	NA	+/ht	+/ht	+
General stage of disability[f]	3	7	4	4	2
Distal sensory loss[g]	+	+	NA	+	+
Spine deformity[h]	−	−	−	+	+
Deep tendon reflexes[i]	−/−	−/−	−/−	−/−	(+)/−
Motor nerves[j]					
Median (≥48/≥8)	39/4.2	ND	35/3.7	36/8.8	39/8.5
Ulnar (≥48/≥8)	ND	ND	35/6.5	34/5.3	33/7.4
Peroneal (≥42/≥5)	29/0.8	ND	27/2.1	NR	29/3.5
Tibial (≥40/≥8)	28/6.3	ND	26/2.5	31/1.0	26/8.8
Sensory nerves[k]					
Median (≥45/≥12)	ND	ND	36/21	40/6	42/17
Ulnar (≥50/≥15)	35/14.3	ND	30/13	37/19	37/10
Superficial peroneal (≥40/≥10)	30/0.7	ND	ND	NR	25/9
Sural (≥42/≥10)	32/2	ND	NR	ND	ND
Sural nerve biopsy	ND	Demyelinating and axonal changes	NA[l]	NA	ND
Muscle biopsy	ND	ND	Neurogenic muscle atrophy	NA	ND

UL, upper limbs; LL, lower limbs; NA, no data available; ND, not done.
[a]Wrist extension: − = no weakness; + = 4/5 on MRC scale; ++ = <4/5 on MRC scale; +++ = complete paralysis.
[b]Ankle dorsiflexion: − = no weakness; + = 4/5 on MRC scale; ++ = <4/5 on MRC scale; +++ = complete paralysis.
[c]− = not affected; + = mild atrophy; ++ = moderate atrophy; +++ = severe atrophy.
[d]− = not affected; + = mild; ++ = severe.
[e]− = no deformity; + = pes cavus; ++ = clubfoot deformity; +++ = surgery required, ht = hammer toes.
[f]0 = normal, 1 = normal walking and running but fatigability and cramps, 2 = normal walking, running and jumping impossible, 3 = abnormal walking without help, 4 = abnormal walking only with simple canes, 5 = abnormal walking only with crutches, 6 = abnormal walking only with a walker, 7 = wheelchair-bound, 8 = bedridden.
[g]− normal sensibility; + = decreased sensibility; ++ = absent sensibility.
[h]− = none; + = mild; ++ = severe; +++ = surgery required.
[i]Upper/lower extremities; + = normal; (+) = decreased; − = areflexia.
[j]Motor nerve conduction velocities (in m/s)/amplitudes of compound motor action potentials (in mV); normal values are given in brackets following the nerve's name; NR, not recordable.
[k]Sensory nerve conduction velocities (in m/s)/sensory nerve action potentials (in μV); normal values are given in brackets following the nerve's name; NR, not recordable.
[l]The biopsy specimens could not be evaluated due to severe traction/fixation artifacts.

Plekhg5$^{\Delta Ex11\text{-}Ex17/\Delta Ex11\text{-}Ex17}$ mice (18). These animals were produced by a cross between animals with *lox*P sites flanking exons 11–17, which contain the RhoGEF catalytic domain considered as a main functional domain of Plekhg5, and a small portion of the PH domain [Fig. 4A, Supplementary Material, Fig. S2 (15,16)] with mice expressing Cre recombinase in their germline [CAG-Cre transgenic mice (19)], thus leading to excision of the targeted region in all mouse tissues, as verified by genomic PCR and RT-PCR (Supplementary Material, Fig. S2). *Plekhg5*$^{\Delta Ex11\text{-}Ex17/\Delta Ex11\text{-}Ex17}$ mice developed normally, without any major phenotype up to adulthood (including the absence of clear neurological symptoms such as tremor, gait instability or changes in open field activity).

We therefore used a combination of electrophysiological and behavioral tests in order to evaluate possible changes in PNS function in *Plekhg5* knockout mice. Electrophysiological evaluation revealed that the MNCV was reduced in 6- and 12-month-old *Plekhg5*$^{\Delta Ex11\text{-}Ex17/\Delta Ex11\text{-}Ex17}$ mice (Fig. 4B) and both proximal and distal compound action potentials (CAPs) were delayed in affected animals at the age of 12 months, while only proximal CAPs were affected at the age of 6 months (Fig. 4C). The reduced velocity (∼6 m/s) was compatible with the relatively mild decrease in MNCVs observed in CMT subjects. *Plekhg5*$^{\Delta Ex11\text{-}Ex17/\Delta Ex11\text{-}Ex17}$ mice were then assessed with the rotarod to test their motor performances. While the affected animals performed slightly less well than control

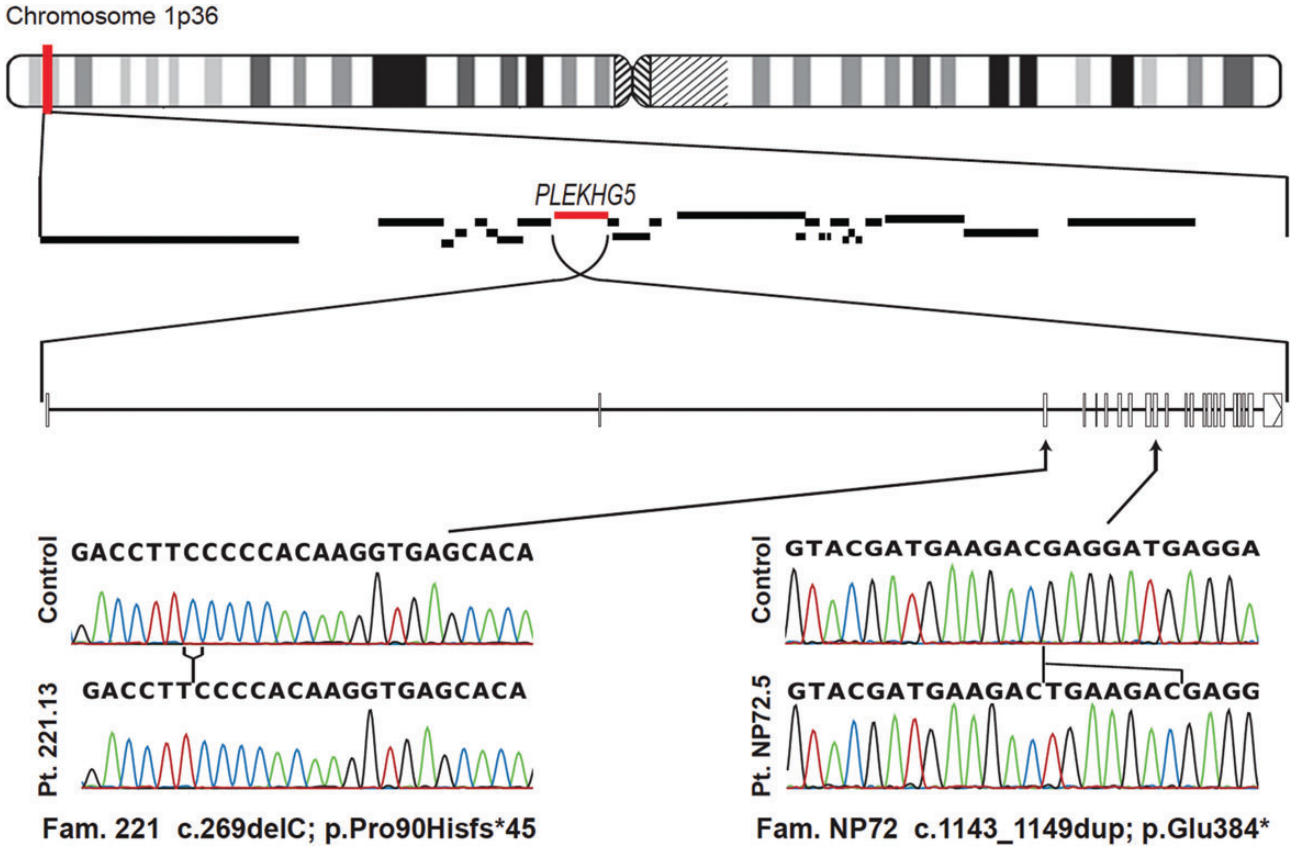

Figure 2. *PLEKHG5* mutations identified in families 221 and NP72. The autozygous region on chromosome 1 common to both families (vertical red bar) contains 25 genes (horizontal black bars), including *PLEKHG5* (horizontal red bar). Chromatograms of DNA from the index case of each family, detailing the mutations identified, are presented, along with control sequences. Genomic structure of *PLEKHG5* and nucleotide numbering is based on reference sequence NM_198681.3. Amino acid numbering is based on reference sequence NP_941374.2.

littermates, this difference did not reach statistical significance (Fig. 4D).

Plekhg5$^{\Delta Ex11\text{-}Ex17/\Delta Ex11\text{-}Ex17}$ mice do not develop lower motor neuron disease

Although clinical characterization of families 221 and NP72 corresponded to an intermediate CMT phenotype, previous data indicated that a missense mutation in *PLEKHG5* leads to a severe form of LMND (12). Thus, we characterized more detail α-motoneurons and neuromuscular junctions (NMJs) in *Plekhg5*$^{\Delta Ex11\text{-}Ex17/\Delta Ex11\text{-}Ex17}$ animals (Fig. 5, Supplementary Material, Fig. S3). Characterization of ventral horn α-motoneurons of the lumbar spinal cord of 6- and 12-month-old *Plekhg5*$^{\Delta Ex11\text{-}Ex17/\Delta Ex11\text{-}Ex17}$ mice failed to reveal any differences in their number or morphological characteristics (Fig. 5A–C; Supplementary Material, Fig. S3). In addition, we did not observe any significant change in the pattern of innervation, change in the NMJ shape or any denervation in the soleus or extensor digitorum longus (EDL) muscles of *Plekhg5*$^{\Delta Ex11\text{-}Ex17/\Delta Ex11\text{-}Ex17}$ mice (Fig. 5D, Supplementary Material, Fig. S3). The absence of changes in α-motoneurons and in NMJ indicated that during the analyzed period (up to 1 year of age), the *Plekhg5*$^{\Delta Ex11\text{-}Ex17/\Delta Ex11\text{-}Ex17}$ mice did not develop detectable signs of LMND.

DISCUSSION

It is presently unknown why some *PLEKHG5* mutations lead to an intermediate CMT neuropathy in humans and mice while others cause severe LMND in affected individuals. The homozygous missense mutation identified in the African family affected by LMND results in an amino acid substitution (p.Phe647Ser) in the pleckstrin homology domain (PH domain, Fig. 4) of PLEKHG5, which affects its subcellular localization and function (12). On the other hand, mutations in CMT families 221 and NP72 most likely result in critically truncated or no protein at all (due to nonsense-mediated decay). The in-frame deletion in the mouse model is also likely to represent a non-functional null allele as it removes the entire Rho guanine nucleotide exchange factor (GEF) catalytic domain that is essential for Plekhg5 to regulate RhoGTPase signaling (15,16).

Importantly, it was previously observed that defects in other GEFs affect the PNS function. Mutations in *FGD4* (MIM 611104) lead to demyelinating Charcot–Marie–Tooth disease CMT4H (MIM 609311) (20–22), while a missense mutation in *ARHGEF10* (Rho guanine nucleotide exchange factor 10; MIM 608136) results in an autosomal-dominant trait with slowed NCV without clinical manifestation (23).

Recent data also indicate that PLEKHG5 may interact with a variety of partners including multiple PDZ domain protein 1

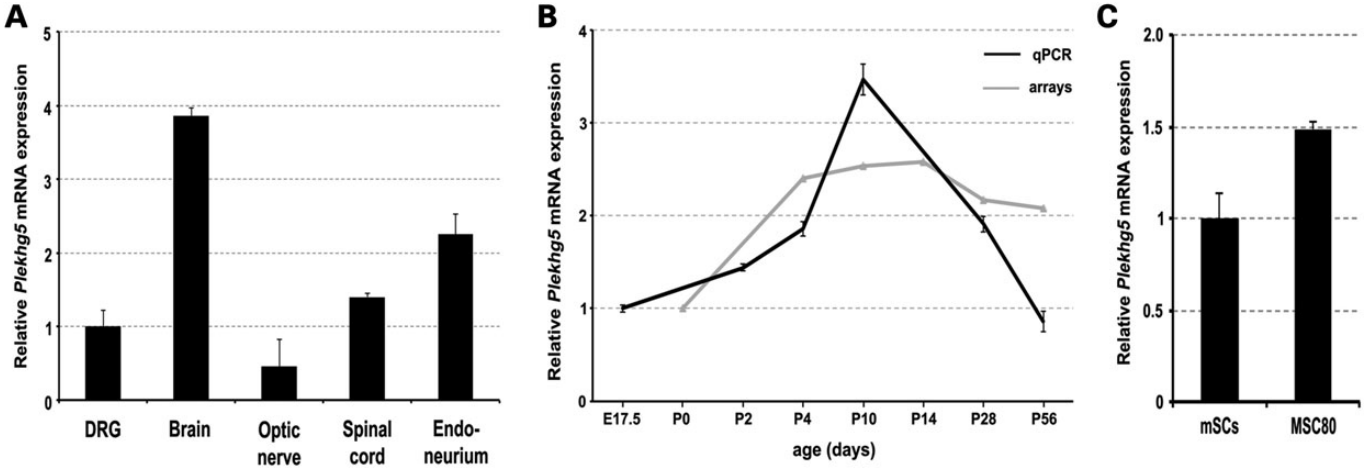

Figure 3. Plekhg5 expression in mouse nervous system. (**A**) The relative level of *Plekhg5* expression was evaluated by quantitative PCR (qPCR) in dorsal root ganglia (DRG), brain, optic nerve, spinal cord and sciatic nerve endoneurium. mRNA levels are presented as fold change over the mRNA level in the DRG. The data represent the mean ± SD of triplicate measurements. (**B**) Relative mRNA levels of *Plekhg5* were determined by qPCR and microarrays (E17, P0, P2, P4 and P10: whole mouse sciatic nerve; P14, P28 and P56: sciatic nerve endoneurium). For each time point, the mRNA levels are presented as fold increase over the mRNA level at E17.5 (for qPCR measurements) or at P0 (for microarray experiments). The qPCR data represent the mean ± SD of triplicate measurements. (**C**) Relative mRNA levels of *Plekhg5* were determined by qPCR in purified mouse Schwann cells (mSCs) and in the mouse SC line (MSC80). The data are represented as fold change over the mRNA levels in mSCs. The presented qPCR results were normalized using *Ube2l3* as the reference gene.

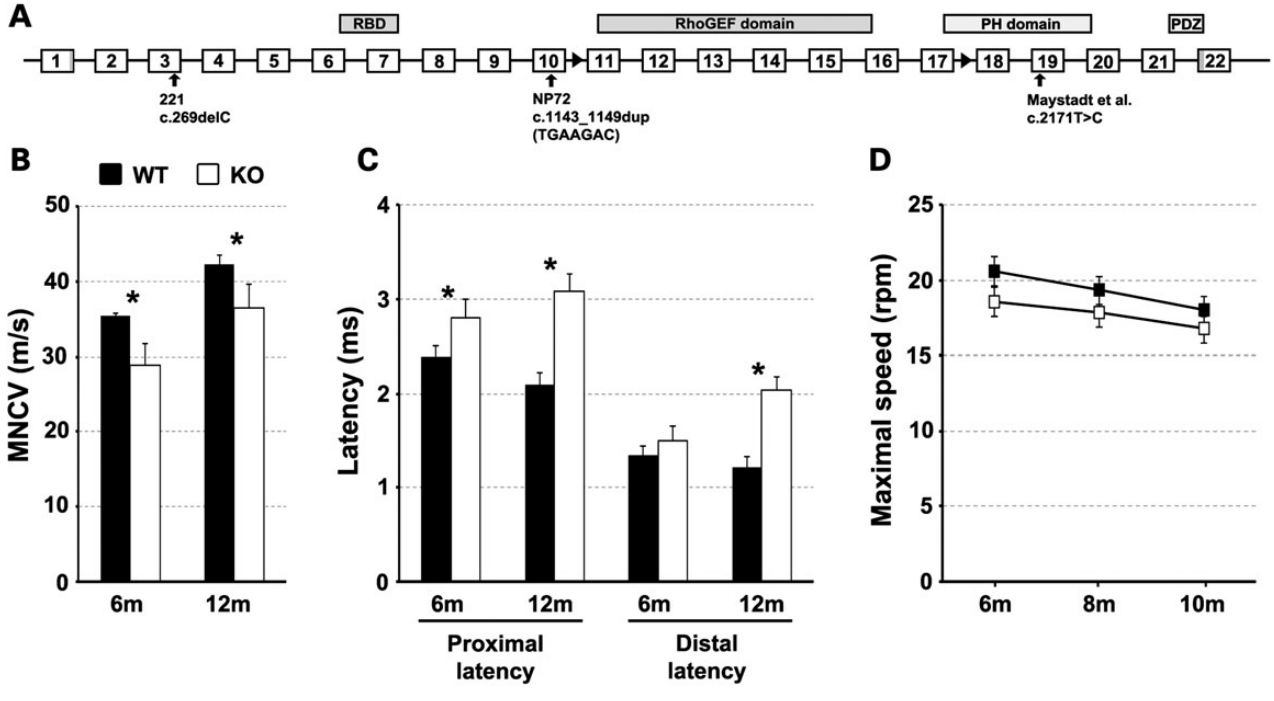

Figure 4. Disruption of Plekhg5 function in mice leads to mild neuropathy. (**A**) Schematic diagram showing the targeted *Plekhg5* allele (based on Ensembl transcript ENSMUST00000118648). Homologous recombination between two loxP sites (black arrowheads positioned between exons 10–11 and 17–18) led to the deletion of exons 11–17 which contain the complete Rho-GEF domain and a small portion of the pleckstrin homology (PH) domain. The deletion of exons 11–17 (816 nucleotides) does not disrupt the reading frame of the truncated mRNA. The position of the previously described missense mutation (12) is indicated as well as the positions of mutations identified in this study. RBD: Ras binding domain; PDZ: Psd95-Dlg1-Zo1 domain (**B**) Electrophysiological characterization of 6- and 12-month-old wild-type (WT, $Plekhg5^{+/+}$) and knockout (KO, $Plekhg5^{\Delta Ex11\text{-}Ex17/\Delta Ex11\text{-}Ex17}$) animals revealed reduced motor nerve conduction velocity (MNCV) in affected mice ($n = 4–5$). (**C**) Both proximal CAP and distal CAP were delayed in affected animals. (**D**) Knockout mice exhibit deficits in rotarod performance test; however, the observed difference does not reach statistical significance. Error bars: SEM, statistically significant differences are indicated by * ($P < 0.05$).

[MUPP1 or MPDZ; MIM 603785 (24,25)], in particular through its PDZ-binding motif that is lost in families 221 and NP72. MUPP1 is one of the proteins involved in epithelial-like polarization of SC (26,27), which is critical for both radial and longitudinal extension of their myelin sheaths (26,28). It is therefore possible that disturbed interactions between PLEKHG5 and

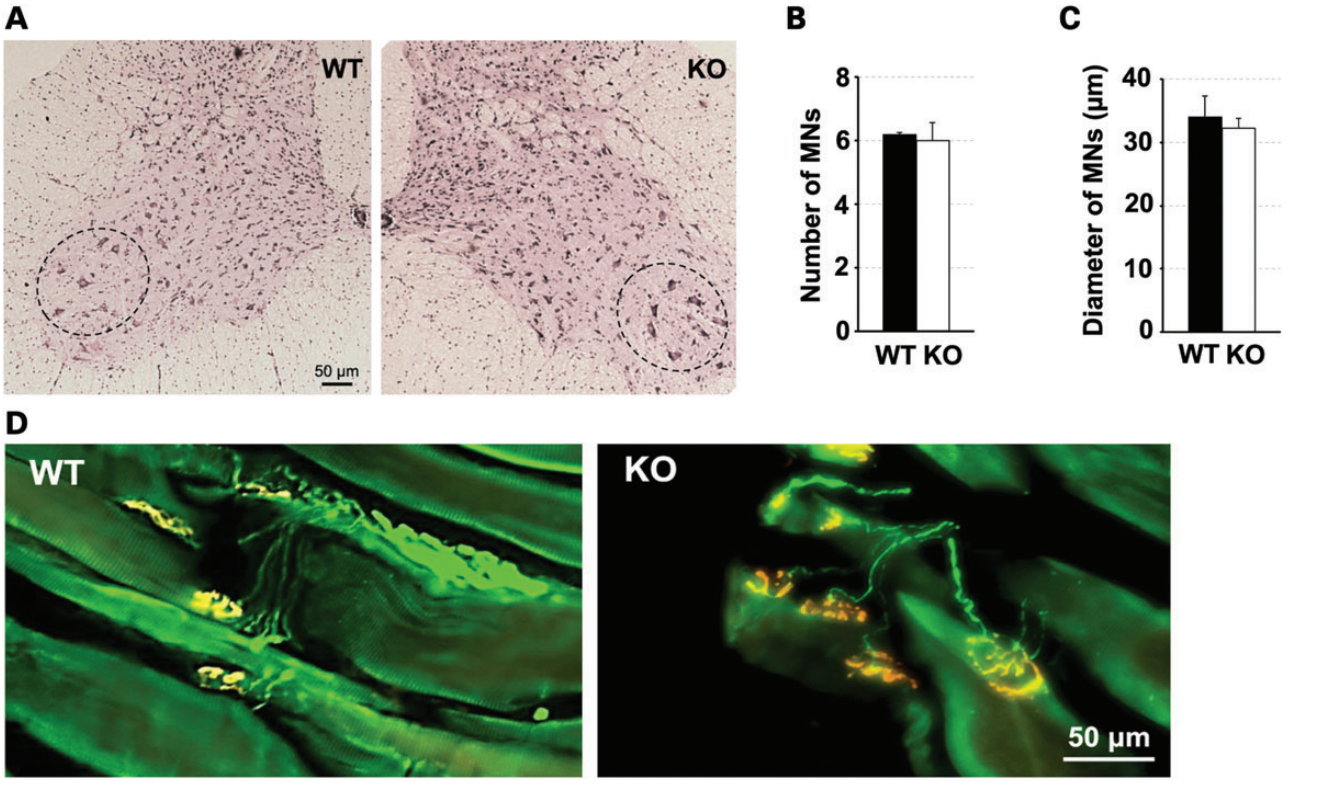

Figure 5. Disruption of Plekhg5 function does not lead to detectable defects in motoneurons or NMJ. (**A**) Characterization of lumbar α-motoneurons in *Plekhg5*$^{\Delta Ex11\text{-}Ex17/\Delta Ex11\text{-}Ex17}$ mice at the age of one year. No difference in the number (**B**) or size (**C**) of α-motoneurons (MN) per ventral horn was detected between control (WT, *Plekhg5*$^{+/+}$) and affected (KO, *Plekhg5*$^{\Delta Ex11\text{-}Ex17/\Delta Ex11\text{-}Ex17}$) animals. (**D**) Confocal images of presynaptic nerve terminals (detected with α-neurofilament antibodies, in green) and postsynaptic endplates (detected with α-bungarotoxin CF594, in red). We did not observe obvious structural abnormalities in the soleus and EDL muscles of *Plekhg5* deficient animals.

its partners could contribute to some of the CMT phenotypes present in families 221 and NP72.

Finally, it was also previously shown that PLEKHG5 is able to activate the nuclear factor κB (NF-κB) signaling pathway (12). Activation of NF-κB signaling pathway was previously shown to play critical roles in both neurons/axons (29) and in SC biology (30). It is therefore possible that disturbed NF-κB signaling contributes to neuronal and/or glial phenotypes caused by mutations in *PLEKHG5*.

To conclude, our results reveal that in addition to severe LMNDs, *PLEKHG5* mutations can also lead to intermediate CMT. While further data are needed, the above-mentioned observations indicate that PLEKHG5 is involved in both glial and neuronal function. Therefore, this gene should be considered in genetic diagnosis in families with clinical pictures compatible with CMT or LMNDs.

MATERIAL AND METHODS

Web resources

Online Mendelian Inheritance in Man (OMIM), http://www.omim.org/.
dbSNP, http://www.ncbi.nlm.nih.gov/SNP.
Exome Variant Server, http://evs.gs.washington.edu/EVS/.
Marshfield Center, http://research.marshfieldclinic.org/genetics.
National Center of Biological Investigation, http://www.ncbi.nlm.nih.gov.
Ensembl, http://www.ensembl.org.
UCSC, http://genome.ucsc.edu.
HomozygosityMapper, http://www.homozygositymapper.org.

Genotyping and linkage analyses

After informed consent was given, blood samples from selected members of the Moroccan and the Portuguese families were obtained. Genomic DNA was extracted using standard procedures. To identify the disease locus in family 221, we perform a genome-wide mapping using 400 microsatellites, spaced 10 cM apart on all chromosomes (ABI-Prism linkage mapping set v2; Applied Biosystems). Several additional microsatellite markers were used to further delimitate the critical interval of segregation of the disease locus. Polymerase chain reaction (PCR) fragments were resolved on an ABI-3730 sequencer (Applied Biosystems) and genotypes were determined with GeneMapper-3.5 (Applied Biosystems). In family NP72, a genome-wide SNP genotyping was carried out using Illumina 660W-Quad microarrays (Illumina). Linkage analyses in family 221 were performed with ALLEGRO 1.2c (31) and in addition we used Merlin 1.1.2 (13) for linkage in both families, with the following parameters: the disease was considered to be a fully penetrant autosomal-recessive trait, with a disease allele frequency of 0.001 in the population and equal

recombination fractions for male and female individuals. We assigned equal frequencies to the alleles observed in both families. For microsatellite markers, genetic distances were taken from the Marshfield Center (http://research.marshfieldclinic.org/genetics) according to the human genome map [available from National Center of Biological Investigation (http://www.ncbi.nlm.nih.gov), Ensembl (http://www.ensembl.org) and UCSC (http://genome.ucsc.edu)]. Homozygosity mapping for family NP72 was performed using HomozygosityMapper [http://www.homozygositymapper.org; (32)]. In order to combine both microsatellite and SNP markers to calculate a joined LOD score under Merlin software, we used the Rutgers Map V3 (GRCh37 patch 4: a third-generation combined linkage-physical map of the human genome) as well as DeCode Map and UniSTS data banks.

DNA sequencing

Primers were designed using Oligo6 (MBI; Molecular Biology Insights, Inc.) to amplify all coding exons of the candidate genes, including exon–intron boundaries. Both strands of the PCR products were subjected to Sanger sequencing with BigDye Terminator chemistry V3.1 (Applied Biosystems) on an ABI 3730 sequencer. Sequence chromatograms were analyzed using SeqScape software version 2.5 (Applied Biosystems).

Plekhg5$^{\Delta Ex11\text{-}Ex17/\Delta Ex11\text{-}Ex17}$ mice genotyping

Plekhg5$^{\Delta Ex11\text{-}Ex17/\Delta Ex11\text{-}Ex17}$ and control (*Plekhg5*$^{+/+}$) mice were genotyped by two separate PCRs amplifying the WT allele and the knockout allele. Primer combinations conKO2/conKO4 and conKO2/ApaIRA were used for amplifying the WT and null alleles, respectively. Primer sequences are available upon request.

Quantitative PCR

Total RNA was isolated from adult (2-months-old) wild-type mice dorsal root ganglia, brain, optic nerve and spinal cord, from sciatic nerves isolated at various developmental time points (E17-P56), from purified mouse SC and MSC80 cells as previously described (33). Two hundred and fifty to 500 ng of total RNA was subjected to reverse transcription using SuperScriptTM III First-Strand Synthesis System for RT-PCR (Life Technologies) following manufacturer's instructions. Resulting cDNA was used as a template for relative quantitation using the ABI Prism 7500 Fast Real-Time PCR System (Life Technologies) as previously described (33). The qPCR results were normalized using *Ube2l3* as the reference gene. Primer sequences are available upon request.

Rota-rod characterization of *Plekhg5*$^{\Delta Ex11\text{-}Ex17/\Delta Ex11\text{-}Ex17}$ mice

All animals were tested during the light phase of the light-dark cycle. At least eight control and eight *Plekhg5*$^{\Delta Ex11\text{-}Ex17/\Delta Ex11\text{-}Ex17}$ mice were tested three times at each time point. Mice were placed on a rod rotating at a speed of 5 rpm (Rotamex-5; Columbus Instruments). Then, the speed was increased by 0.5 rpm every 5 s. The speed at which mice fell off the rod was recorded for each trial.

Electrophysiological characterization of *Plekhg5*$^{\Delta Ex11\text{-}Ex17/\Delta Ex11\text{-}Ex17}$ mice

Electrophysiological characterization of 6- and 12-month-old control and *Plekhg5*$^{\Delta Ex11\text{-}Ex17/\Delta Ex11\text{-}Ex17}$ mice was performed as previously described (34). All animals were anesthetized with a mixture of 10 ml/g ketanarkon 100 (1 mg/ml; Streuli) and 0.1% Rompun (Bayer) in PBS. The left and right sciatic nerves were stimulated at the sciatic notch and distally at the ankle via bipolar electrodes with supramaximal square-wave pulses (5 V) of 0.05 ms and the latencies of the compound muscle action potentials were recorded.

Motoneuron analysis

Animals were deeply anesthetized with isoflurane and decapitated. The entire lumbar region of the spinal cord was dissected out and post-fixed in 4% PFA PBS (0.1 M, pH 7.4) solution overnight at 4°C. Tissues were cryoprotected by immersion for 48 h in a 20% sucrose PBS solution at 4°C. Tissues were embedded in O.C.T (VWR) on dry ice. We then performed experiment as previously described with few minor modifications (35). Serial sections (thickness: 16 μm) of the spinal cord were collected and motoneurons were stained with hematoxylin/eosin. Motoneurons (with a diameter over 25 μm; α-motoneurons) in the ventrolateral quarter of both sides were counted every fifth sections for a total of 20 sections per spinal cord.

Whole mount immunohistochemistry of soleus and EDL NMJs

Animals were deeply anesthetized with isoflurane and decapitated. The slow-twitch muscle soleus and the fast-twitch muscle EDL were collected on both sides, pinned on a Sylgard-coated dish, fixed 30 min in 4% PFA PBS solution and then incubated in a sucrose 20% PBS solution before OCT embedding. Fifteen micrometer sections were prepared and permeabilized 2 h in a 5% BSA 0.5% Triton PBS solution. Presynaptic component of the NMJ and SC morphology was revealed by S100 (1:250; Dako) and α-neurofilament stainings (1:200 NF145; Millipore) overnight and followed by 2 h incubation with goat anti-rabbit Alexa 488 secondary antibody (1:200; Invitrogen). To label the post-synaptic endplates, tissues were then exposed to α-bungarotoxin CF594 (Biotium) for 1 h. To finish, muscles sections were washed with PBS and mounted in Mowiol (Calbiochem). Sections were imaged with a Zeiss Axiovision. Innervated or denervated endplates were counted on 15 μm Z-stacks with a ×20 magnification.

SUPPLEMENTARY MATERIAL

Supplementary Material is available at *HMG* online.

ACKNOWLEDGEMENTS

The authors are grateful to Emeline Mundwiller (*Institut du Cerveau et de la Moelle épinière*, Genotyping and Sequencing facility) and the DNA and Cell bank of CRICM for technical assistance. We especially thank all individuals and family members who participated in this research.

Conflict of Interest statement. None declared.

FUNDING

This work was supported by the University of Lausanne, the Gebert Rüf Foundation GRS-046/09 (to C.R., R.C. and J.S.), the GUS-Rare Diseases Institute (to G.S.), the Association française contre les myopathies (AFM; to H.A.) and the Swiss National Science Foundation (grant 31003A_135735/1 to R.C., and grants 320030-121929 and 310030_138346 to C.R.).

REFERENCES

1. Skre, H. (1974) Genetic and clinical aspects of Charcot-Marie-Tooth's disease. *Clin. Genet.*, **6**, 98–118.
2. Thomas, P.K. and Harding, A.E. (1993) Inherited neuropathies: the interface between molecular genetics and pathology. *Brain Pathol.*, **3**, 129–133.
3. Shy, M.E., Blake, J., Krajewski, K., Fuerst, D.R., Laura, M., Hahn, A.F., Li, J., Lewis, R.A. and Reilly, M. (2005) Reliability and validity of the CMT neuropathy score as a measure of disability. *Neurology*, **64**, 1209–1214.
4. Thomas, P.K. and Calne, D.B. (1974) Motor nerve conduction velocity in peroneal muscular atrophy: evidence for genetic heterogeneity. *J. Neurol. Neurosurg. Psychiatry*, **37**, 68–75.
5. Bouche, P., Gherardi, R., Cathala, H.P., Lhermitte, F. and Castaigne, P. (1983) Peroneal muscular atrophy. Part 1. Clinical and electrophysiological study. *J. Neurol. Sci.*, **61**, 389–399.
6. Rossi, A., Paradiso, C., Cioni, R., Rizzuto, N. and Guazzi, G. (1985) Charcot-Marie-Tooth disease: study of a large kinship with an intermediate form. *J. Neurol.*, **232**, 91–98.
7. Reilly, M.M. and Shy, M.E. (2009) Diagnosis and new treatments in genetic neuropathies. *J. Neurol. Neurosurg. Psychiatry*, **80**, 1304–1314.
8. Saporta, A.S., Sottile, S.L., Miller, L.J., Feely, S.M., Siskind, C.E. and Shy, M.E. (2011) Charcot-Marie-Tooth disease subtypes and genetic testing strategies. *Ann. Neurol.*, **69**, 22–33.
9. Madrid, R., Bradley, W.G. and Davis, C.J. (1977) The peroneal muscular atrophy syndrome. Clinical, genetic, electrophysiological and nerve biopsy studies. Part 2. Observations on pathological changes in sural nerve biopsies. *J. Neurol. Sci.*, **32**, 91–122.
10. Gherardi, R., Bouche, P., Escourolle, R. and Hauw, J.J. (1983) Peroneal muscular atrophy. Part 2. Nerve biopsy studies. *J. Neurol. Sci.*, **61**, 401–416.
11. Azzedine, H., Senderek, J., Rivolta, C. and Chrast, R. (2012) Molecular genetics of Charcot-Marie-Tooth disease: from genes to genomes. *Mol. Syndromol.*, **3**, 204–214.
12. Maystadt, I., Rezsohazy, R., Barkats, M., Duque, S., Vannuffel, P., Remacle, S., Lambert, B., Najimi, M., Sokal, E., Munnich, A. *et al.* (2007) The nuclear factor kappaB-activator gene PLEKHG5 is mutated in a form of autosomal recessive lower motor neuron disease with childhood onset. *Am. J. Hum. Genet.*, **81**, 67–76.
13. Abecasis, G.R., Cherny, S.S., Cookson, W.O. and Cardon, L.R. (2002) Merlin—rapid analysis of dense genetic maps using sparse gene flow trees. *Nat. Genet.*, **30**, 97–101.
14. Verdier, V., Csardi, G., de Preux-Charles, A.S., Medard, J.J., Smit, A.B., Verheijen, M.H., Bergmann, S. and Chrast, R. (2012) Aging of myelinating glial cells predominantly affects lipid metabolism and immune response pathways. *Glia*, **60**, 751–760.
15. De Toledo, M., Coulon, V., Schmidt, S., Fort, P. and Blangy, A. (2001) The gene for a new brain specific RhoA exchange factor maps to the highly unstable chromosomal region 1p36.2–1p36.3. *Oncogene*, **20**, 7307–7317.
16. Marx, R., Henderson, J., Wang, J. and Baraban, J.M. (2005) Tech: a RhoA GEF selectively expressed in hippocampal and cortical neurons. *J. Neurochem.*, **92**, 850–858.
17. Verheijen, M.H., Chrast, R., Burrola, P. and Lemke, G. (2003) Local regulation of fat metabolism in peripheral nerves. *Genes Dev.*, **17**, 2450–2464.
18. Garnaas, M.K., Moodie, K.L., Liu, M.L., Samant, G.V., Li, K., Marx, R., Baraban, J.M., Horowitz, A. and Ramchandran, R. (2008) Syx, a RhoA guanine exchange factor, is essential for angiogenesis *in Vivo*. *Circ. Res.*, **103**, 710–716.
19. Sakai, K. and Miyazaki, J. (1997) A transgenic mouse line that retains Cre recombinase activity in mature oocytes irrespective of the cre transgene transmission. *Biochem. Biophys. Res. Commun.*, **237**, 318–324.
20. Stendel, C., Roos, A., Deconinck, T., Pereira, J., Castagner, F., Niemann, A., Kirschner, J., Korinthenberg, R., Ketelsen, U.P., Battaloglu, E. *et al.* (2007) Peripheral nerve demyelination caused by a mutant Rho GTPase guanine nucleotide exchange factor, frabin/FGD4. *Am. J. Hum. Genet.*, **81**, 158–164.
21. Delague, V., Jacquier, A., Hamadouche, T., Poitelon, Y., Baudot, C., Boccaccio, I., Chouery, E., Chaouch, M., Kassouri, N., Jabbour, R. *et al.* (2007) Mutations in FGD4 encoding the Rho GDP/GTP exchange factor FRABIN cause autosomal recessive Charcot-Marie-Tooth type 4H. *Am. J. Hum. Genet.*, **81**, 1–16.
22. Horn, M., Baumann, R., Pereira, J.A., Sidiropoulos, P.N., Somandin, C., Welzl, H., Stendel, C., Luhmann, T., Wessig, C., Toyka, K.V. *et al.* (2012) Myelin is dependent on the Charcot-Marie-Tooth Type 4H disease culprit protein FRABIN/FGD4 in Schwann cells. *Brain*, **135**, 3567–3583.
23. Verhoeven, K., De Jonghe, P., Van de Putte, T., Nelis, E., Zwijsen, A., Verpoorten, N., De Vriendt, E., Jacobs, A., Van Gerwen, V., Francis, A. *et al.* (2003) Slowed conduction and thin myelination of peripheral nerves associated with mutant rho Guanine-nucleotide exchange factor 10. *Am. J. Hum. Genet.*, **73**, 926–932.
24. Estevez, M.A., Henderson, J.A., Ahn, D., Zhu, X.R., Poschmann, G., Lubbert, H., Marx, R. and Baraban, J.M. (2008) The neuronal RhoA GEF, Tech, interacts with the synaptic multi-PDZ-domain-containing protein, MUPP1. *J. Neurochem.*, **106**, 1287–1297.
25. Ngok, S.P., Geyer, R., Liu, M., Kourtidis, A., Agrawal, S., Wu, C., Seerapu, H.R., Lewis-Tuffin, L.J., Moodie, K.L., Huveldt, D. *et al.* (2012) VEGF and Angiopoietin-1 exert opposing effects on cell junctions by regulating the Rho GEF Syx. *J. Cell Biol.*, **199**, 1103–1115.
26. Ozcelik, M., Cotter, L., Jacob, C., Pereira, J.A., Relvas, J.B., Suter, U. and Tricaud, N. (2010) Pals1 is a major regulator of the epithelial-like polarization and the extension of the myelin sheath in peripheral nerves. *J. Neurosci.*, **30**, 4120–4131.
27. Poliak, S., Matlis, S., Ullmer, C., Scherer, S.S. and Peles, E. (2002) Distinct claudins and associated PDZ proteins form different autotypic tight junctions in myelinating Schwann cells. *J. Cell Biol.*, **159**, 361–372.
28. Cotter, L., Ozcelik, M., Jacob, C., Pereira, J.A., Locher, V., Baumann, R., Relvas, J.B., Suter, U. and Tricaud, N. (2010) Dlg1-PTEN interaction regulates myelin thickness to prevent damaging peripheral nerve overmyelination. *Science*, **328**, 1415–1418.
29. Gutierrez, H. and Davies, A.M. (2011) Regulation of neural process growth, elaboration and structural plasticity by NF-kappaB. *Trends Neurosci.*, **34**, 316–325.
30. Nickols, J.C., Valentine, W., Kanwal, S. and Carter, B.D. (2003) Activation of the transcription factor NF-kappaB in Schwann cells is required for peripheral myelin formation. *Nat. Neurosci.*, **6**, 161–167.
31. Gudbjartsson, D.F., Jonasson, K., Frigge, M.L. and Kong, A. (2000) Allegro, a new computer program for multipoint linkage analysis. *Nat. Genet.*, **25**, 12–13.
32. Seelow, D., Schuelke, M., Hildebrandt, F. and Nurnberg, P. (2009) HomozygosityMapper—an interactive approach to homozygosity mapping. *Nucleic Acids Res.*, **37**, W593– W 599.
33. de Preux, A.S., Goosen, K., Zhang, W., Sima, A.A., Shimano, H., Ouwens, D.M., Diamant, M., Hillebrands, J.L., Rozing, J., Lemke, G. *et al.* (2007) SREBP-1c expression in Schwann cells is affected by diabetes and nutritional status. *Mol. Cell. Neurosci.*, **35**, 525–534.
34. de Preux Charles, A.S., Verdier, V., Zenker, J., Peter, B., Medard, J.J., Kuntzer, T., Beckmann, J.S., Bergmann, S. and Chrast, R. (2010) Global transcriptional programs in peripheral nerve endoneurium and DRG are resistant to the onset of type 1 diabetic neuropathy in Ins2 mice. *PLoS ONE*, **5**, e10832.
35. Chai, R.J., Vukovic, J., Dunlop, S., Grounds, M.D. and Shavlakadze, T. (2011) Striking denervation of neuromuscular junctions without lumbar motoneuron loss in geriatric mouse muscle. *PLoS ONE*, **6**, e28090.